International Journal of
Turbomachinery Propulsion and Power

MDPI

Article

Effect of Different Subgrid-Scale Models and Inflow Turbulence Conditions on the Boundary Layer Transition in a Transonic Linear Turbine Cascade

Ettore Bertolini [1,*], Paul Pieringer [2] and Wolfgang Sanz [1]

[1] Institute of Thermal Turbomachinery and Machine Dynamics, Graz University of Technology, 8010 Graz, Austria; wolfgang.sanz@tugraz.at
[2] ABES Pircher and Partner GmbH, 8010 Graz, Austria; paul.pieringer@abes-austria.com
* Correspondence: ettore.bertolini@tugraz.at

Abstract: The aim of this work is to study the influence of different subgrid-scale (SGS) closure models and inflow turbulence conditions on the boundary layer transition on the suction side of a highly loaded transonic turbine cascade in the presence of high free-stream turbulence using large eddy simulations (LES) of the MUR237 test case. For the numerical simulations, the MUR237 flow case was considered and the incoming free-stream turbulence was reproduced using the synthetic eddy method (SEM). The boundary layer transition on the blade suction side was found to be significantly influenced by the choice of the SGS closure model and the SEM parameters. These two aspects were carefully evaluated in this work. Initially, the influence of three different closure models (Smagorinsky, WALE, and subgrid-scale kinetic energy model) was evaluated. Among them, the WALE SGS closure model performed best compared to the Smagorinsky and KEM models and, for this reason, was used in the following analysis. Finally, different values of the turbulence length scale, eddies density, and inlet turbulence for the SEM were evaluated. As shown by the results, among the different parameters, the choice of the turbulence length scale plays a major role in the transition onset on the blade suction side.

Keywords: LES; laminar-to-turbulent transition; subgrid-scale model; synthetic eddy method

check for updates

Citation: Bertolini, E.; Pieringer, P.; Sanz, W. Effect of Different Subgrid-Scale Models and Inflow Turbulence Conditions on the Boundary Layer Transition in a Transonic Linear Turbine Cascade. *Int. J. Turbomach. Propuls. Power* **2021**, *6*, 35. https://doi.org/10.3390/ijtpp6030035

Academic Editor: Antoine Dazin

Received: 19 May 2021
Accepted: 18 August 2021
Published: 27 August 2021

1. Introduction

In modern aero engines, the turbine stages have to deal with extreme conditions due to the presence of high pressures, high temperatures, and high levels of turbulence. In order to ensure the performance and the lifetime of the components, precise knowledge and control of the flow field inside the machine is required. Particularly critical is the region of the flow closest to the solid surfaces. This region is called the boundary layer (BL), and it is here that viscous effects drive the exchanges of energy and momentum. The boundary layer can be both laminar and turbulent, and this has a great influence on the transport processes such as wall friction and heat transfer. Furthermore, the ability of the boundary layer to remain attached to the blades in the condition of adverse pressure gradients changes dramatically from laminar to turbulent. Therefore, the control of the boundary layer becomes essential in modern aero engines where high loads and high efficiency are required from every stage.

Much research has been undertaken in the last few decades in order to understand all the complex mechanisms occurring in the boundary layer region. Besides the experimental approach, the numerical solution of the Navier–Stokes (NS) equations has also been used since it can provide a priori useful information for the designers. Consequently, a substantial amount of numerical models has been developed and refined in order to accurately predict the evolution of the boundary layer. While RANS models played a big role concerning simulations of near-wall flows, more recently, thanks to the fast growth of computational resources, more accurate numerical models such as large eddy simulation (LES) and direct numerical simulation (DNS), which were considered almost impossible to use a decade ago for engine-relevant flow conditions, are becoming more and more popular. Among the three, LES seems to be especially attractive due to a lower computational cost compared to DNS and better accuracy and adaptability in comparison with RANS, making it a valuable choice not only in research fields, but also in industrial ones.

One of the biggest challenges for LES when dealing with turbomachinery flows is the prediction of the laminar-to-turbulent transition on the blade surface in the presence of free-stream turbulence. The incoming turbulence has a great impact on the BL evolution and needs to be carefully modeled in order to reach accurate results. However, the specification of the inlet flow data is a bit more complex and challenging in LES compared to RANS since an unsteady turbulence velocity signal has to be superimposed at the inlet boundary in order to reproduce the turbulence statistics of the real flow. Dhamankar et al. [1] provided an overview of the different approaches used for reproducing turbulence. Among the different methods, the synthetic eddy method (SEM) of Jarrin et al. [2] was chosen in this work since it can be used to describe a large number of inlet turbulence conditions in terms of turbulence length scale, anisotropy, and intensity with a relatively low computational cost and a good replicability of the turbulence statistics. Furthermore, it is easy to change the inflow boundary conditions since the method does not require precursor simulations.

The ability of LES to predict the BL transition on a highly loaded turbine blade in the presence of inlet turbulence was investigated in the works of [3–7]. In these works, the flow case investigated was the MUR cascade tested at the von Karman Institute for Fluid Dynamics [8]. The cascade was composed of a linear arrangement of five blades, where the central one was instrumented for both pressure and heat transfer measurements. In the cascade, the influence of free-stream turbulence, the free-stream Reynolds number, and the Mach number on the boundary layer transition and on the heat transfer on the blade was evaluated. Different methods for reproducing the inflow turbulence statistics and different LES setups were used by every author. However, all the numerical configurations exhibited weaknesses in some flow configurations, showing that a reliable prediction of the BL laminar-to-turbulent transition is still a challenge. In the work of Jee et al. [7] in particular, it was found that the boundary layer transition on the blade suction side is significantly influenced by the choice of the subgrid-scale (SGS) closure model and the SEM parameters.

The aim of this paper is to investigate the influence of different LES setups on the boundary layer transition on the blade suction side of a MUR cascade in the presence of synthetic inlet turbulence. For the simulations, the in-house code LINARS was used. The inflow turbulence is described using the SEM routine proposed by [2], and the numerical simulations refer to the MUR237 flow case.

The paper is arranged as follows. Firstly, the influence of three different closure models is evaluated. Starting from the results of [7], the standard Smagorinsky model is compared to the WALE model and the one-equation subgrid-scale kinetic energy model (KEM). Afterwards, the influence of the SEM parameters such as the turbulence intensity, turbulence length scale, and number of turbulent eddies is investigated.

2. Numerical Method

2.1. Flow Case

The flow case investigated in the simulations was the MUR237 test case. This flow case is part of a campaign of measurements (MUR132, MUR218, and MUR237), where the influence of the inflow turbulence intensity on the heat transfer and boundary layer transition on the blade surface was evaluated. The cascade counts in total 5 blades with a chord length, blade height, and blade pitch of 67.647 mm, 100 mm, and 57.5 mm, respectively. The main flow parameters can be found in Table 1. MUR237 involves a higher level (6%) of inflow turbulence and an earlier laminar-to-turbulent transition of the boundary layer on the suction side of the blade compared to the MUR218 (4%) and MUR132 (0.8%) flow cases.

Table 1. Flow parameters and boundary conditions for the numerical investigation.

MUR237			
Parameter	**Symbol**	**Value**	
Total temperature inlet	T_{1tot}	417.3	K
Static temperature inlet	T_{1s}	415.43	K
Total pressure inlet	p_{1tot}	1.753	bar
Static pressure inlet	p_{1s}	1.726	bar
Velocity inlet	v_1	61.29	m/s
Static pressure outlet	p_{2s}	1.179	bar
Wall temperature	T_{wall}	299.85	K
Reynolds number outlet	Re_{out}	1.0×10^6	-
Freestream turbulence	Tu	6.0%	-
Incidence angle	β_1	0	deg
Exit Mach number	M_{2is}	0.775	-

2.2. Computational Mesh

For the MUR237 flow case, the flow at midspan has been proven to be independent of the hub and shroud secondary vortices and reasonably periodic in the circumferential direction for the central vane [8]. Hence, the numerical grid considers only one vane channel, and only part of the entire blade span is considered. The numerical span was equal to 10% of the entire blade height since it was shown in the work of [5] that by a further increase of the numerical span, no significant improvement in the results can be achieved. Figure 1 displays the computational grid used. A configuration with O-blocks around the blade was used in order to guarantee higher accuracy close to the blade wall while maintaining a low number of grid points in the free-stream region where such a grid resolution is not needed. As can be seen in the black frame in Figure 1, the number of grid points along the streamwise direction was doubled moving towards the blade surface from one O-block to the consecutive one. A total of 3 layers of O-blocks was used. At the outlet, two coarser blocks were added in order to increase the dissipation of the flow structures of the wake and reduce the reflections at the outlet boundary. The grid counts a total of 38M grid points, and it was designed in order to achieve a maximum value of y^+, x^+, and z^+ of 1.2, 40, and 30, respectively. Furthermore, in the free-stream region, the maximum grid spacing was equal to 0.3 mm.

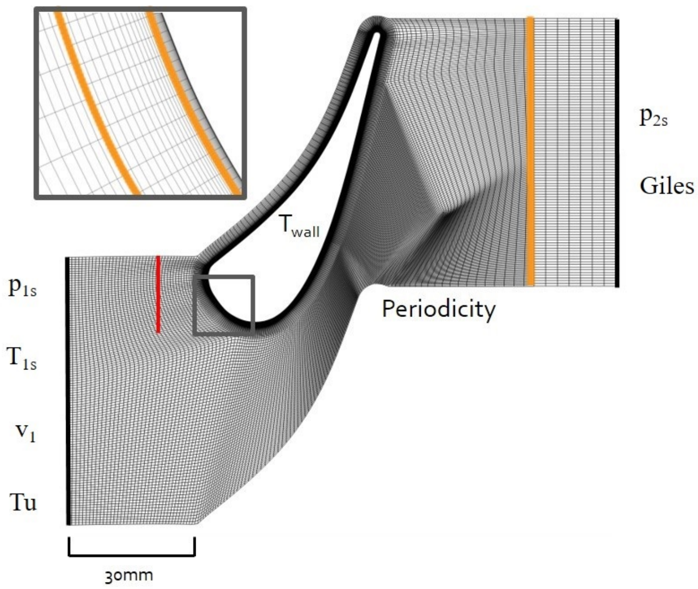

Figure 1. Computational grid and O-blocks.

2.3. Boundary Conditions

At the inlet and outlet, the boundary conditions were assigned according to Figure 1 the parameters in Table 1. At the outlet, the static pressure was assigned, as well as a Giles nonreflective boundary condition [9] in order to improve the stability of the simulations. At the inlet, the static temperature, static pressure, and mean velocity were imposed, whereas the inlet turbulence intensity was prescribed using the SEM. At the blade wall, a constant temperature equal to 299.85 K was set. Between the O-blocks around the blade and the coarser blocks in the outer layers, an interpolation of second-order was used to connect the faces. Further information about the interpolation used can be found in [7]. Finally, periodicity was used in the circumferential and spanwise direction.

2.4. Numerical Schemes

For the time iteration, the fourth-order explicit Runge–Kutta method (RK4) was used with a time step of 4×10^{-9} s and a maximum value of $CFL < 1$. For the computation of the cell fluxes, a weighted essentially nonoscillatory (WENO) scheme was used since it was proven by [10] to give better performance compared to the central schemes and the TVD schemes in terms of numerical stability and dissipation.

2.5. Computational Time

The simulations were performing using the in-house code LINARS. The numerical domain was split into several blocks for parallel computing and a total of 160 cores was used for each simulation. Approximately 2.5×10^5 core hours were needed to carry out every simulation.

2.6. Subgrid-Scale Models

In this work, three different SGS models were used: Smagorinsky–Lilly, wall-adapting local eddy-viscosity (WALE), and the one-equation subgrid-scale kinetic energy model (KEM).

2.6.1. Smagorinsky–Lilly Model

The standard Smagorinsky–Lilly model was used in this paper. Lilly originally found a value of the Smagorinsky coefficient C_s equal to 0.17 [11]. This value gives good results for isotropic turbulence in the free-stream region, but it introduces a too high dissipation when dealing with near-wall flows. For this type of flow, a value equal to 0.1 is usually recommended. However, in [7] it was found that with a Smagorinsky coefficient equal to 0.1, the boundary layer evolution on the MUR blade could not be accurately predicted because the closure model was still too dissipative. Different values of the Smagorinsky coefficient were tested for the MUR132 flow case, and a value equal to 0.05 was found to give the best performance. For this reason, this value was also used in this work.

A damping function acting on the Smagorinsky length scale was also applied in order to reduce the viscosity in the near-wall region:

$$\ell_s = min(\kappa d, C_s V^{1/3}) \tag{1}$$

where d is the distance from the solid wall, κ represents the von Karman constant $\kappa = 0.41$, and V is the volume of the computational cell.

2.6.2. WALE Model

The WALE model [12] is a subgrid-scale model based on the square of the velocity gradient tensor. Compared to the standard Smagorinsky–Lilly model, in the WALE model the eddy viscosity with this formulation goes naturally to zero close to the wall, and it is also zero in the case of pure shear stress. The eddy viscosity is rewritten as:

$$\mu_t = \rho L_s^2 \frac{(S_{ij}^d S_{ij}^d)^{3/2}}{(\overline{S}_{ij}\overline{S}_{ij})^{5/2} + (\overline{S}_{ij}\overline{S}_{ij})^{5/4}} \tag{2}$$

$\overline{S}_{ij}$ is the rate-of-strain tensor for the resolved scale, which can be expressed as:

$$\overline{S}_{ij} = \frac{1}{2}\left(\frac{\partial \overline{u_i}}{\partial x_j} + \frac{\partial \overline{u_j}}{\partial x_i}\right) \tag{3}$$

whereas the mixing length L_s and the parameter S_{ij}^d are defined respectively as:

$$L_s = min(\kappa d, C_\omega V^{1/3}) \tag{4}$$

$$S_{ij}^d = \frac{\partial \overline{u_i}}{\partial x_j} \tag{5}$$

The coefficient C_ω was set equal to 0.325 since this value has been proven to produce satisfactory results for a wide range of flows.

2.6.3. KEM Model

In the KEM closure model, the eddy viscosity is expressed as:

$$\mu_t = C_k \sqrt{k_{sgs}} V^{1/3} \tag{6}$$

where k_{sgs} is the kinetic energy related to the subgrid scales of turbulence, and it is obtained from the additional transport equation:

$$\frac{\partial k_{sgs}}{\partial t} + \overline{u}_j \frac{\partial k_{sgs}}{\partial x_j} = -\tau_{ij}\frac{\partial \overline{u}_i}{\partial x_j} - C_c \frac{k_{sgs}^{3/2}}{\Delta} + \frac{\partial}{\partial x_j}\left[\left(\frac{\nu_k}{\sigma_k} + \nu\right)\frac{\partial k_{sgs}}{\partial x_j}\right] \tag{7}$$

In the equation, the terms on the right-hand side are, respectively, production, dissipation, and diffusion. The constants were set according to the work of [13] as $C_k = 0.05$, $C_c = 1.0$, and $\sigma_k = 1.0$, whereas Δ was obtained from the cell volume as $\Delta = V^{1/3}$. Finally, the inlet condition for the subgrid-scale kinetic energy was set equal to 6% of the inlet turbulence kinetic energy.

2.7. SEM

The main principles of the SEM are as follows. The eddies that constitute a set of velocity fluctuations are contained in a box outside of the computational domain. The eddies are defined in the box by the coordinates of their center, their velocity fluctuation distribution, and their size. The location of the eddies is randomly defined, as well as the direction of the fluctuation, which is assigned using a random variable taken from the distribution $\{-1; 1\}$ with equal probability to take one or the other value. The eddies are then convected from the SEM box to the computational domain by using Taylor's frozen hypothesis [2].

The setup of the SEM used in this work was the same as in [7], and the main points are recalled here. An isotropic turbulent inflow was considered, so the intensity of the turbulence fluctuations was the same for the three velocity components and equal to the product between the average inlet velocity and the turbulence intensity ($a_{ii} = TuU$). The dimension of the box was the same in the circumferential and spanwise direction as the inlet boundary of the main computational domain, whereas the length in the streamwise direction was found by multiplying the average inlet velocity by a time constant τ as $L_x = \tau U$. Finally, the number of eddies was found as recommended in the work of [14] by dividing the volume of the SEM box (V_{SEM}) by the cube of the turbulence length scale (σ) as:

$$N = V_{SEM}/\sigma^3 \tag{8}$$

It is important to mention that when all the eddies inside the SEM box are transported inside the computational domain, a new SEM box is generated. The new SEM box is defined by a new set of random eddies. The random eddies were picked from an external pool previously generated with MATLAB. The total number of eddies contained in the pool was chosen in order to avoid the time periodicity of the inlet turbulence in the time frame of the simulation. As a consequence, τ did not have any influence on the generated turbulence, but it was only used to build an initial SEM box used for flow visualization and for checking the correctness of the turbulence statistics.

Different SEM boxes were defined for this investigation. The main parameters of each of them are displayed in Table 2. In all boxes, 6.5% inlet turbulence was prescribed apart from SEM5T8, where 8% was used. The turbulence length scale was equal to 5 mm for SEM5 and SEM5T8, 3 mm for SEM3 and SEM3N4, and 2 mm for SEM2. The time constant τ was chosen in order to have enough eddies in the streamwise direction inside the SEM box and good turbulence statistics. The number of eddies was then obtained from Equation (8), apart from SEM3N4, where the number of eddies that was prescribed was 4-times larger. Finally, in the last column of Table 2, the density of the eddies in the SEM box is reported. As can be seen, the density of the eddies increased by reducing the turbulence length scale.

Table 2. SEM box parameters.

Name	σ	Tu	τ	N	N/V_{SEM}
SEM2	2 (mm)	6.5 (%)	0.0006 (s)	2643 (-)	0.125 ($1/mm^3$)
SEM3	3 (mm)	6.5 (%)	0.006 (s)	7831 (-)	0.037 ($1/mm^3$)
SEM5	5 (mm)	6.5 (%)	0.01 (s)	2819 (-)	0.008 ($1/mm^3$)
SEM3N4	3 (mm)	6.5 (%)	0.0005 (s)	2610 (-)	0.148 ($1/mm^3$)
SEM5T8	5 (mm)	8.0 (%)	0.01 (s)	2819 (-)	0.008 ($1/mm^3$)

For the SGS closure model comparison, only the SEM5 box was used for the definition of the inlet turbulence. For the investigation of the influence of the inlet turbulence length scale, SEM2, SEM3, and SEM5 were used. Regarding the influence of the number of eddies, the simulation using SEM3 was compared to the one with SEM3N4. Finally, SEM5 and SEM5T8 were compared in order to investigate the effect of the turbulence intensity.

3. Results

In this section, the results of the current investigation are presented and discussed. The experimental convective heat transfer coefficient (h) on the blade surface was compared with the predicted one of the LES simulations. In order to obtain h, the main flow parameters were recorded every 5000 iterations. Then, an average in time was performed, as well as along the spanwise direction. In order to prove that the solution had converged, the integral of the convective heat transfer coefficient over a region on the suction side of the blade close to the trailing edge was evaluated over time. After convergence was reached, 250,000 time steps were performed, and a total number of 50 samples were taken. h was then obtained by the definition:

$$h = \frac{\dot{q}_{wall}}{T_{1tot} - T_{wall}} \quad (9)$$

where $\dot{q}_{wall}$, T_{1tot}, and T_{wall} are the wall heat flux, total inlet temperature, and wall temperature, respectively. Finally, in order to compare with the experiments, the convective heat transfer coefficient was plotted along the curvilinear abscissa (S) for both the pressure side (PS) and suction side (SS). In the heat transfer measurements of the MUR test case, an uncertainty of 5% was estimated, so it was taken into account in the graphs using error bars.

3.1. SGS Closure Model Influence

The convective heat transfer coefficient predicted by the three different SGS models for the MUR237 test case is displayed in Figure 2. Looking at the suction side (SS), the three models reached similar levels at the blade leading edge (0 mm $<$ S $<$ 20 mm). Starting from $S = 20$ mm and up to $S = 58$ mm, WALE and SMAG predicted slightly lower levels of h compared to KEM. However, starting from $S = 58$, this trend changed, and both WALE and SMAG predicted a sudden increase of h due to the laminar-to-turbulent transition of the boundary layer (a visualization of the boundary layer for the WALE simulation is provided in Figure 6). On the other hand, KEM did not show a complete transition, and consequently, lower levels of h were reached. Focusing now on the pressure side, even though the heat transfer was similar at the blade leading edge, starting from the position $S = -5$, the three models exhibited some differences. KEM in particular predicted the highest levels of h all over the PS, whereas SMAG and WALE showed similar behavior, with the latter giving slightly lower levels of heat transfer.

To further analyze the differences between the tested SGS models, the wall shear stress on the blade wall was also computed. Looking at Figure 3, contrary to what was found for the convective heat transfer, the three models showed very similar levels of wall shear stress at the blade pressure side, with the WALE giving slightly lower values compared to KEM and SMAG. Concerning the SS, the predicted wall shear stress was similar in the first part of the suction side up to $S = 20$ mm. From this point on, some small differences could be found within the region 20 mm $<$ S $<$ 60 mm, but it was again closer to the trailing edge where the greatest deviations between the models could be found due to a different prediction of the laminar-to-turbulent transition.

In Figure 4, the velocity profiles are reported. The velocity profiles were extrapolated in two locations on the SS at $S = 60$ mm (beginning of the laminar-to-turbulence transition) and $S = 80$ mm (more turbulent BL) and one on the PS at $S = -20$ mm. In the graphs, theoretical solutions of the flat plate flow for both the viscous sublayer (dashed line) and the logarithmic law of the wall (dashed-dotted line) are also included. Generally, the velocity profiles of the different SGS models were very similar when the boundary layer was laminar (positions $S = -20$ mm and $S = 60$ mm), and they matched the viscous sublayer theoretical shape well. On the contrary, at position $S = 80$ mm, the models behaved very differently. The KEM velocity profile was still laminar compared to the ones of WALE and SMAG, which showed a more turbulent profile. Among the three models, WALE seemed to perform best in both the viscous sublayer and in the log-law region.

Looking again at position $S = 80$, none of the SGS models matched the turbulence velocity profile given by the logarithmic law of the wall. In order to find the reason for the discrepancy, the velocity profiles were also drawn in this location for a RANS solution with the k-ω SST model combined with the γ-Re_θ transition model. As can be seen in Figure 4, the RANS model predicted the theoretical line in the log-law region better compared to the LES models. Looking now at the heat transfer coefficient in Figure 2, it can be clearly seen that the RANS model exhibited a much more rapid transition compared to LES and also predicted a much higher level of convective heat transfer once that transition had occurred. This indicates that the LES models did not predict a full transition of the boundary layer which could explain the discrepancy in the log-law region of the velocity profiles and in the heat transfer.

Overall, by comparing the experimental and the numerical results, h was underpredicted in all three LES simulations, and this difference was larger in the aft part of the blade SS, where the transition occurred much more downstream than in the experiments. Furthermore, as was previously found in [6,7], the predicted heat transfer better agree with the experimental results of the MUR218 flow case where a lower level of turbulence (4%) at the inlet was generated (see Figure 2).

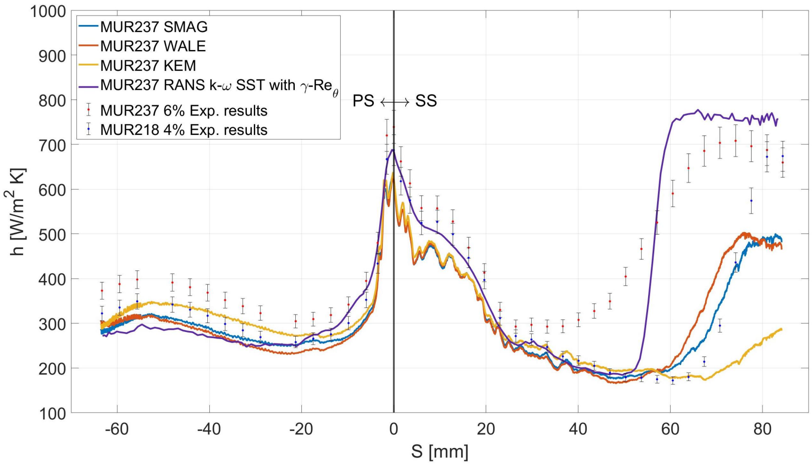

Figure 2. Influence of the SGS closure models: convective heat transfer coefficient.

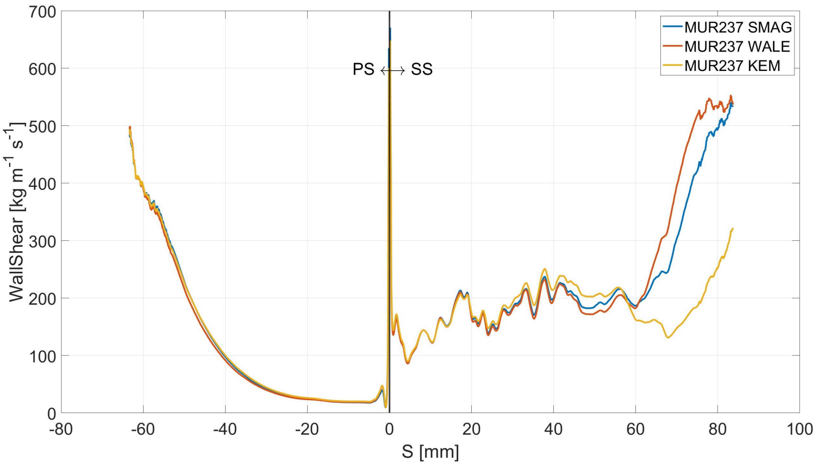

Figure 3. Influence of the SGS closure models: wall shear stress.

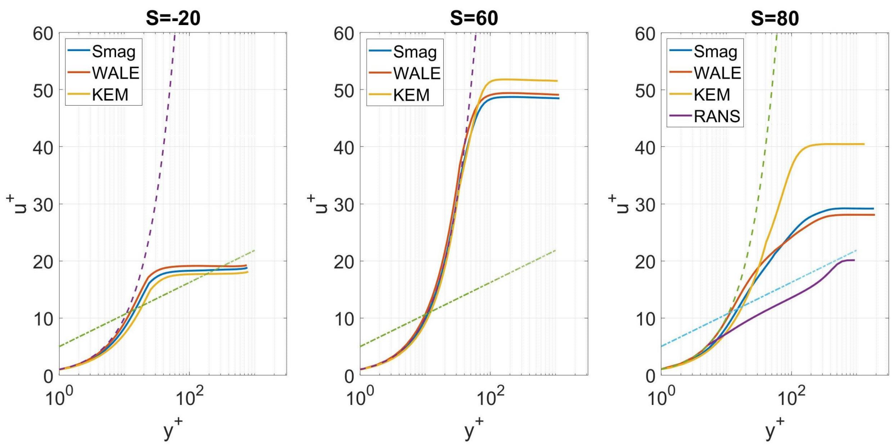

Figure 4. Influence of the SGS closure models: velocity profile.

In [7], some open questions remained regarding the origin of the deviation between the experimental and numerical results and whether it was connected to the chosen SGS closure model or the SEM parameters. From these results, it can be concluded that the choice of the SGS model influences the prediction of the heat transfer on the blade surface at both the pressure and suction side, whereas on the SS the influence seems to be restricted to the BL laminar-to-turbulent transition region when looking at the wall shear stress. KEM had more subgrid-scale viscosity than WALE and SMAG, and this caused a suppression of the laminar-to-turbulent transition on the blade SS. WALE and SMAG gave similar results, but the first one seems to be slightly less dissipative than SMAG and also performed better in the subviscous layer of the boundary layer. Therefore, for this reason, it was used in the further investigations of this work.

3.2. Influence of SEM Box Parameters

As the next step, the impact of the SEM parameters on the convective heat transfer and the laminar-to-turbulent BL transition is discussed. In particular, the influence of the turbulence length scale, the number of eddies prescribed in the SEM box, and the turbulence intensity are treated separately.

3.2.1. Turbulence Length Scale

In the experiments, no information regarding the turbulence length scales was given. However, the mixing length is well known to have a great influence on the boundary layer transition. In the works of [5,6,15], a deep discussion on the choice of the mixing length for the simulation of the MUR flow case can be found, and the typical values chosen in their investigations varied between 1.5 and 8 mm. According to the range of values found in the literature, three different turbulence length scales were chosen, 2 mm, 3 mm, and 5 mm, for the current investigation.

For this set of simulations, the WALE model was used, whereas turbulence was prescribed by the 2 mm, 3 mm, and 5 mm turbulence length scale cases, respectively, using SEM2, SEM3, and SEM5 (see Table 2). Looking at the convective heat transfer in Figure 5, some differences can be already noticed at the blade leading edge where larger values of heat transfer can be found for the 3 mm and 2 mm flow cases. On the blade pressure side, the predicted heat transfer was very similar between SEM5 and SEM3, whereas SEM2 predicted slightly higher levels of h from $S = -20$ mm to the trailing edge. On the suction side, the differences were more remarkable. Starting from the leading edge and up to $S = 20$ mm, the heat transfer was closer to the experimental results for the 3 mm flow case, whereas only slight differences could be found between 2 mm and 5 mm. Between $S = 20$ mm and $S = 40$ mm, it seemed that h converged to similar levels for all three turbulence length scales, but starting from $S = 40$ mm, the heat transfer for SEM3 rose considerably, showing a much earlier laminar-to-turbulent transition compared to SEM5 and SEM2, where the transition onset was at $S = 60$ mm. By comparing the numerical and experimental results, it is interesting that an inlet turbulence length scale equal to 3 mm remarkably improved the results, whereas a larger (5 mm) and smaller (2 mm) length scale showed similar, but worse results.

In order to better understand the reason for such a difference in the results between the 3 mm and the 5 mm flow cases, the interaction between the incoming turbulence and the boundary layer was investigated by looking at the instantaneous flow field around the blade. As can be seen by the isosurfaces of the Q criterion colored by the velocity magnitude in Figure 6, the density of eddies in the near-wall region was much larger when a 3 mm length scale was prescribed. It has to be remembered that the number of eddies was chosen according to Equation (8), so that a lower density of eddies was expected when a larger turbulence length scale was used (see Table 2). As Figure 6 suggests, this had a great impact on the boundary layer even though the same turbulence intensity was prescribed at the inlet boundary. By observing the contour of spanwise vorticity, it can also be clearly seen that the 3 mm inlet turbulence influenced the pressure side BL as well as the suction side, where the onset of transition occurred much earlier. On the other hand, even though the density of the eddies was the highest for the 2 mm flow case, a later transition was found compared to the 3 mm flow case and similar to the 5 mm case. This was probably caused by a higher dissipation of the smaller turbulence length scale that occurred in the free-stream region. Due to the faster dissipation, the eddies that hit the boundary layer were weaker and could not properly trigger the BL transition.

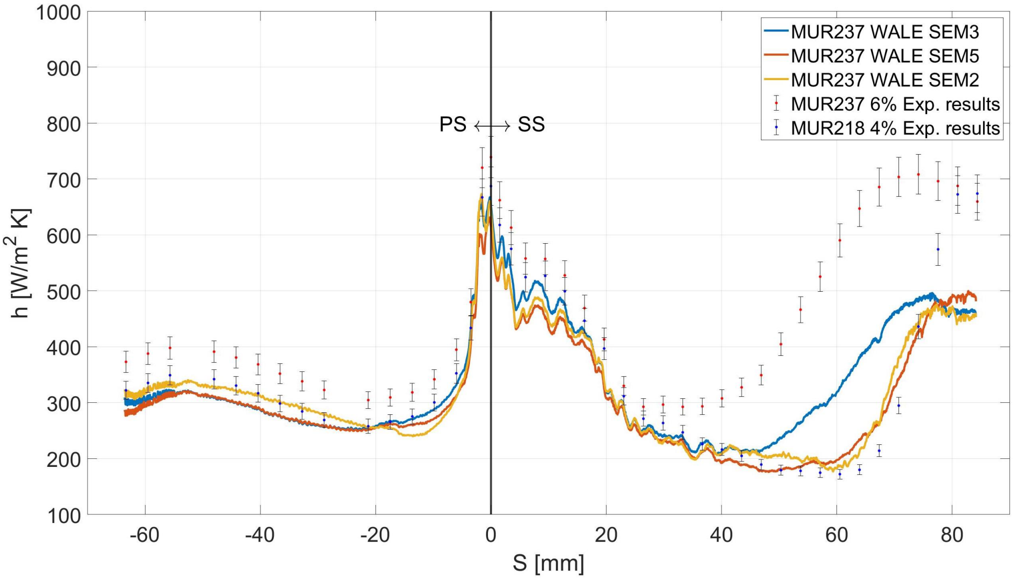

Figure 5. Influence of the turbulence length scales: convective heat transfer coefficient.

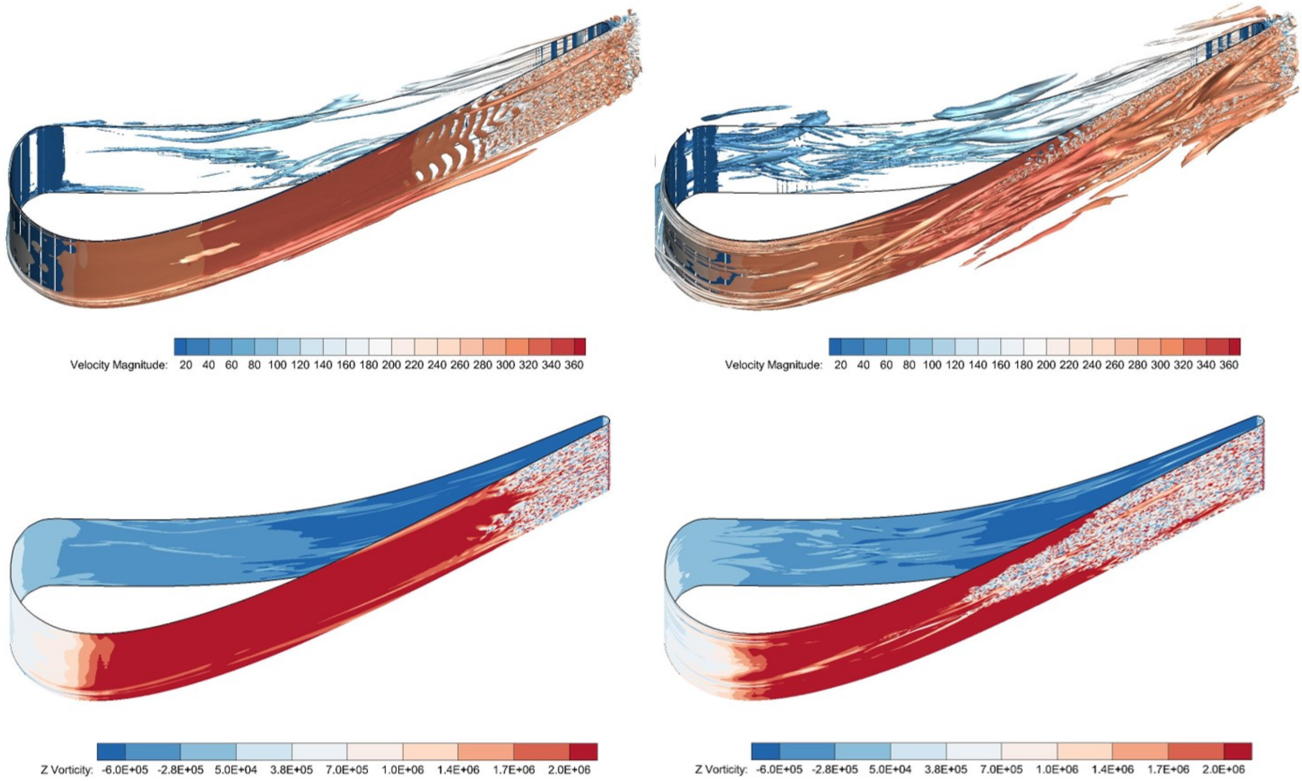

Figure 6. Interaction of the incoming turbulent eddies with the boundary layer for the 3 mm and 5 mm cases: isosurfaces of $Q = 1 \times 10^8$ colored by velocity magnitude (**top**) and the contour of spanwise vorticity at 1×10^{-5} mm from the blade surface (**bottom**).

3.2.2. Number of Eddies

In Figure 7, the results of the investigation regarding the influence of the number of eddies in the SEM box are displayed. Increasing the number of eddies by a factor of four from SEM3 to SEM3N4 led to a degradation of the result quality, and in particular, a later onset of transition could be found. A comparison of the turbulence kinetic energy (TKE) level between the two flow cases was performed at 10 mm upstream the leading edge of the blade (see the red plane in Figure 1). SEM3N4 showed at this point almost 6% less TKE compared to SEM3 despite having the same value at the inlet boundary. When a larger number of eddies was used compared to the recommended one of Equation (8), more regions exist inside the SEM box where the eddies overlap. This could lead to a deterioration of the turbulence fluctuations and, consequently, to a faster dissipation of the TKE along the streamwise direction.

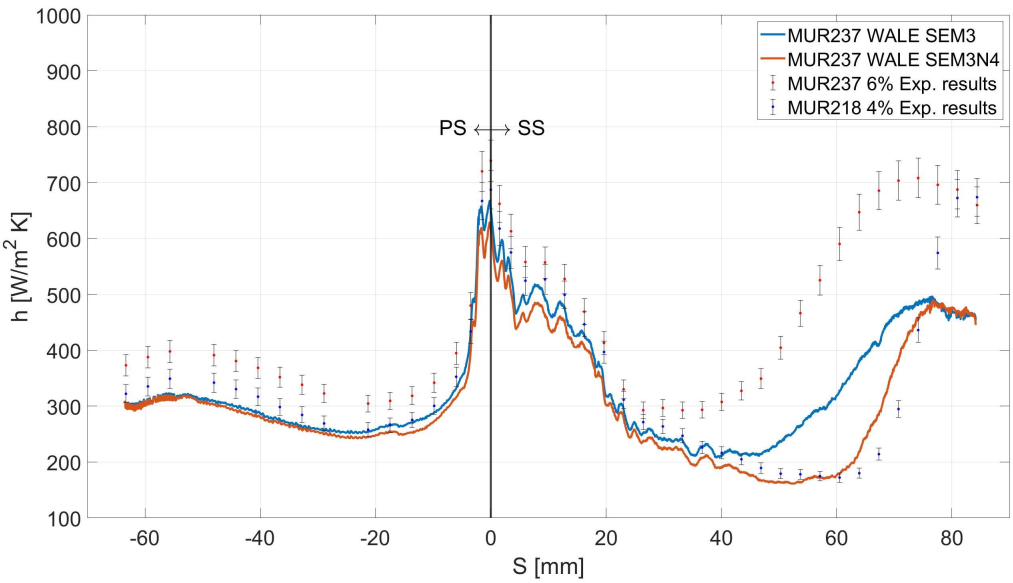

Figure 7. Influence of the number of eddies: convective heat transfer coefficient.

3.2.3. Turbulent Intensity

Looking at Figure 8, it can be seen that by increasing the turbulence intensity from 6% to 8% for the 5 mm flow case, very few changes in the convective heat transfer coefficient could be found. The onset of transition on the SS remains unchanged between the two flow cases, although a slightly higher level of h was predicted for the higher turbulence case between $S = 0$ and $S = 20$ mm. However, a faster transition could be observed for SEM5T8.

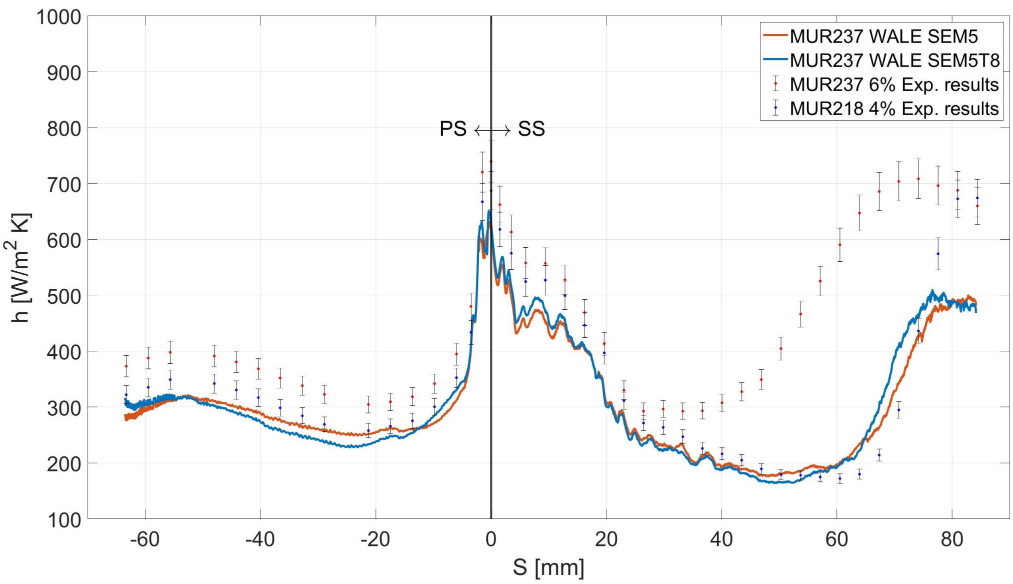

Figure 8. Influence of the turbulence intensity: convective heat transfer coefficient.

4. Conclusions

In this work, the influence of different LES setups on the boundary layer transition on the blade suction side of a highly loaded turbine cascade in the presence of synthetic inlet turbulence was discussed. From the investigation with the different SGS closure models (SMAG, WALE, and KEM), it was found that the choice of the SGS model influenced the prediction of the heat transfer at both pressure and suction side of the blade. In particular, the main differences existed in the region of the suction side where the laminar-to-turbulent transition of the boundary layer occurred. Here, KEM proved to be much more dissipative than WALE and SMAG, and this caused a suppression of the laminar-to-turbulent transition. WALE and SMAG gave similar results, but the first one seemed to be slightly less dissipative than SMAG and also performed better in the subviscous layer of the boundary layer. Regarding the influence of the SEM parameters for prescribing the inlet turbulence such as the turbulence intensity, turbulence length scale, and number of turbulent eddies, it was found that the turbulence length scale had a greater impact on the boundary layer transition and consequently on the heat transfer compared to the other two. In particular, with a turbulence length scale equal to 3 mm, a remarkable improvement of the numerical results compared to the experimental one for the convective heat transfer coefficient was found, especially for the transition onset location. Finally, the increased turbulence intensity seems not to have great impact on the heat transfer, whereas a larger number of eddies in the SEM box resulted in a decrease of turbulence and a deterioration of the turbulence statistics.

Author Contributions: Conceptualization, E.B., P.P. and W.S.; methodology, E.B., P.P. and W.S.; software, E.B., P.P. and W.S.; validation, E.B.; formal analysis, E.B. and W.S.; investigation, E.B. and W.S.; resources, E.B., P.P. and W.S.; data curation, E.B. and W.S.; writing—original draft preparation, E.B.; writing—review and editing, E.B., P.P. and W.S.; visualization, E.B.; supervision, W.S.; project administration, W.S.; funding acquisition, W.S. All authors read and agreed to the published version of the manuscript.

Funding: This research was conducted in the framework of the project ALESIA (Advanced Large Eddy Simulation in Aeroengines) supported by the Austrian Federal Ministry for Transport, Innovation and Technology within the Austrian Aeronautics Program TAKE OFF.

Institutional Review Board Statement: Not applicable.

Informed Consent Statement: Not applicable.

Data Availability Statement: Not applicable.

Acknowledgments: The authors would like to acknowledge the use of the HPC resources provided by the ZID of Graz University of Technology.

Conflicts of Interest: The authors declare no conflict of interest.

Abbreviations

The following abbreviations are used in this manuscript:

BL	Boundary Layer
CFL	Courant–Friedrichs–Lewy
DNS	Direct numerical simulation
KEM	Subgrid-scale Kinetic energy model
LES	Large eddy simulation
NS	Navier–Stokes
PS	Pressure side
RANS	Reynolds-averaged Navier–Stokes
SGS	Subgrid scale
SEM	Synthetic eddy method
SMAG	Smagorinsky
SS	Suction side
WALE	Wall-adapting local eddy-viscosity

Roman Symbols

C_c	Constant of the KEM model
C_k	Constant of the KEM model
C_s	Smagorinsky coefficient
C_ω	Constant of the WALE model
d	Distance to the wall
ℓ_s	Smagorinsky length scale
h	Convective heat transfer coefficient
L_S	Mixing length
k_{sgs}	Kinetic energy of the the subgrid scale
M_{2is}	Isentropic Mach number outlet
p_{1tot}	Inlet total pressure
p_{1s}	Inlet static pressure
p_{2s}	Outlet static pressure
$\dot{q}_{wall}$	Wall heat flux
Re_{out}	Reynolds number at the outlet
S	Curvilinear coordinate
$\overline{S}_{ij}$	Rate-of-strain tensor
S^d_{ij}	Rate-of-strain tensor for the resolved scale
T_{1s}	Inlet static temperature
T_{1tot}	Inlet total temperature
T_{wall}	Wall temperature
Tu	Turbulence level
$u+$	Dimensionless velocity
v_1	Inlet velocity
V	Volume of the computational cell
V_{SEM}	Volume of the SEM box
$y+$	Dimensionless wall distance

Greek Symbols

κ	von Karman constant
μ_t	Eddy viscosity
ρ	Density
σ	Turbulent length scale of the SEM box
σ_k	Constant of the KEM model
τ	Time constant of the SEM box

References

1. Dhamankar, N.; Blaisdell, G.; Lyrintzis, A. An Overview of Turbulent Inflow Boundary Conditions for Large Eddy Simulations (Invited). In Proceedings of the 22nd AIAA Computational Fluid Dynamics Conference, Dallas, TX, USA, 22–26 June 2015. [CrossRef]
2. Jarrin, N.; Benhamadouche, S.; Laurence, D.; Prosser, R. A synthetic-eddy-method for generating inflow conditions for large-eddy simulation. *Int. J. Heat Fluid Flow* **2006**, *27*, 585–593. [CrossRef]
3. Bhaskaran, R.; Lele, S.K.; Eaton, J.K.; Moin, P. *Large Eddy Simulation of High Pressure Turbine Cascade*; Stanford University: Stanford, CA, USA, 2010.
4. Gourdain, N.; Gicquel, L.Y.M.; Morata, E. Comparison of RANS simulation and les for the prediction of heat transfer in a highly loaded turbine guide vane. In Proceedings of the 9th European Conference on Turbomachinery: Fluid Dynamics and Thermodynamics, Istanbul, Turkey, 21–25 March 2011; Volume 2, pp. 847–862. [CrossRef]
5. Morata, E.C.; Gourdain, N.; Duchaine, F.; Gicquel, L. Effects of free-stream turbulence on high pressure turbine blade heat transfer predicted by structured and unstructured LES. *Int. J. Heat Mass Transf.* **2012**, *55*, 5754–5768. [CrossRef]
6. Jee, S.; Joo, J.; Medic, G. Large-Eddy Simulation of a High-Pressure Turbine Vane with Inlet Turbulence. In Proceedings of the ASME Turbo Expo 2016, Seoul, Korea, 13–17 June 2016; Volume 2D; Turbomachinery, GT2016–56980. [CrossRef]
7. Bertolini, E.; Pieringer, P.; Sanz, W. Large Eddy Simulation of a Transonic Linear Cascade with Synthetic Inlet Turbulence. In Proceedings of the ASME Turbo Expo 2020, London, UK, 22–26 June 2020; Volume 2C; Turbomachinery, GT2020–14461.
8. Arts, T.; Lambert de Rouvroit, M.; Rutherford, A.W.; Von Karman Institute for Fluid Dynamics. *Aero-Thermal Investigation of a Highly Loaded Transonic Linear Turbine Guide Vane Cascade: A Test Case for Inviscid and Viscous Flow Computations*; Technical Note Von Karman Institute for Fluid Dynamics; von Karman Institute for Fluid Dynamics: Sint-Genesius-Rode, Belgium, 1990.

9. Giles, M.B. Nonreflecting boundary conditions for Euler equation calculations. *AIAA J.* **1990**, *28*, 2050–2058. [CrossRef]
10. Bertolini, E.; Pieringer, P.; Sanz, W. Prediction of Separated Flow Transition Using LES and Transitional RANS Model. In Proceedings of the ASME Turbo Expo 2019, Phoenix, AZ, USA, 17–21 June 2019; Volume 2C; Turbomachinery, GT2019–90214.
11. Pope, S.B. *Turbulent Flows*; Cambridge University Press: Cambridge, UK, 2000.
12. Franck, N.; Ducros, F. Subgrid-Scale Stress Modelling Based on the Square of the Velocity Gradient Tensor. *Flow Turbul. Combust.* **1999**, *62*, 183–200. [CrossRef]
13. Yoshizawa, A.; Horiuti, K. A Statistically-Derived Subgrid-Scale Kinetic Energy Model for the Large-Eddy Simulation of Turbulent Flows. *J. Phys. Soc. Jpn.* **1985**, *54*, 2834–2839. [CrossRef]
14. Poletto, R.; Craft, T.; Revell, A. A New Divergence Free Synthetic Eddy Method for the Reproduction of Inlet Flow Conditions for LES. *Flow Turbul. Combust.* **2013**, *91*, 1–21. [CrossRef]
15. Liu, Y. Aerodynamics and heat transfer predictions in a highly loaded turbine blade. *Int. J. Heat Fluid Flow* **2007**, *28*, 932–937. [CrossRef]